WS13 A02

A Fast 3-D Free-surface Topography Method for Acoustic Full-waveform Inversion

M.J. Huiskes* (Shell Global Solutions International BV), R.E. Plessix (Shell Global Solutions International BV) & W.A. Mulder (Shell GSI BV & Delft University of Technology)

SUMMARY

We propose a finite-difference scheme for the simulation of seismic waves interacting with 3-D free-surface topography. The intended application is velocity model building by acoustic full-waveform inversion (FWI). The scheme follows an immersed boundary approach for wave equations in the first-order stress-velocity formulation, discretized on a standard staggered grid. Our scheme employs modified 1-D stencils rather than a full 3-D field wavefield extension at the free surface. Although this decreases the accuracy, it improves the scheme's simplicity and robustness. To avoid stability problems, points close to the zero-pressure boundary must be excluded. The scheme, and its adjoint, have been tested by tilted geometry tests and by comparison to a finite-element method. We present a first test result of full-waveform inversion with the new scheme.

Introduction

We propose a finite-difference scheme for the simulation of seismic waves interacting with 3-D free-surface topography. The intended application is velocity model building by acoustic full-waveform inversion (FWI). The application of existing schemes to FWI has a considerable cost, in particular due to assumptions regarding the underlying discretization and the required number of samples per wavelength. Also, several existing approaches are not stable under all circumstances for standard staggered grid discretizations — the method of choice in many highly optimized FWI codes.

Approaches based on adding an air/vacuum layer with topography represented in a staircase-like fashion, such as the direct vacuum method (e.g. Bohlen and Saenger, 2006) or the approach of Robertsson (1996) require a relatively large number of grid points per wavelength (c.f. Lombard et al., 2008).

Grid deformation approaches are based on a transformation of the depth coordinate such that the 3-D topography becomes flat in the transformed coordinates. This results in schemes with grid points directly on the free surface. However, the transformed wave equation requires additional derivative operators with respect to the transformed depth coordinate that are not present in the original wave equations. These can be computed by wavefield interpolation (Hestholm, 2003) or by using a discretization with additional field components per grid point, for instance, by means of a fully staggered grid (FSG). De la Puente et al. (2014) use the deformation method with FSG. They also adopt a mimetic approach to preserve high-order derivative approximations near the free surface.

For immersed boundary methods (Lombard et al., 2008), the free surface does not have to coincide with the discretization grid. Wavefields are extended beyond the free surface such that regular high-order discretization stencils may be used to approximate derivatives near the free surface. The method described in Lombard et al. (2008) is not stable for standard staggered grids. It is implemented using a high-order, single-grid ADER method.

Next to the mentioned finite-difference schemes, variational approaches based on finite-element discretizations are natural candidates for handling 3-D topography, if the mesh is adapted to the boundary. The spectral-element method on hexahedra (Komatitsch and Vilotte, 1998, e.g.) may offer relatively good performance and accuracy for application in FWI (Brossier et al., 2014). Tetrahedra offer more gridding flexibility and are a good alternative (Zhebel et al., 2014).

For general elastic modelling, in particular the simulation of surface waves along a 3-D topography, more expensive variational approaches or finite-difference schemes based on fully staggered grids may be required to achieve sufficient accuracy. However, for the case of acoustic FWI, we propose a more affordable immersed boundary scheme. It employs modified 1-D stencils near the free surface, is stable on a standard-staggered grid (SSG) with high-order derivative stencils, and is sufficiently accurate at a small number, 4 to 6, of grid points per wavelength.

Method

We consider the 3-D acoustic wave equation in the stress-velocity formulation. The fully second-order formulation requires a slightly different approach and will not be discussed here. For the sake of exposition, we consider the 2-D case:

$$\partial_t p = -c_p^2 \rho (\partial_x v_x + \partial_z v_z), \quad \rho\, \partial_t v_x = -\partial_x p, \quad \rho\, \partial_t v_z = -\partial_z p. \tag{1}$$

Here, $p(t,x,z)$ is pressure as a function of time t and position (x,z), $v_x(t,x,z)$ and $v_z(t,x,z)$ are the horizontal and vertical velocity, respectively, ρ is the density, and c_p the P-wave sound speed. At the free-surface boundary, $\Gamma : (x(\tau), z(\tau))$, the usual zero traction condition reduces to zero pressure, $p(x(\tau), z(\tau), t) = 0$, in the acoustic case. We discretize (1) on a standard staggered grid. The free surface does not have to coincide with the discretization grid.

The main challenge in formulating a finite-difference scheme is the accurate approximation of the spatial derivatives in (1) for grid points near the free surface. To this end, we use an immersed boundary approach in which the wavefields are extended beyond the free surface such that we can still use regular high-order derivative stencils for the derivative approximation. In our approach, we restrict ourselves to constructing 1-D extensions of the wavefield. The extended or virtual wavefield is only constructed

in the direction where we need the spatial derivative by combining the free-surface conditions with interpolation through a number of interior values. As we consider only 1-D extensions, an exterior grid point can sometimes be assigned several 'virtual' values if that point is required for derivatives in different directions. Figure 1 illustrates the approximation procedure.

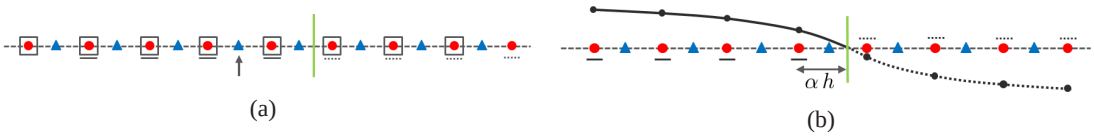

Figure 1 *(a) Pressure (●) derivative approximation at a particle velocity (▲) grid point (↑) using a regular (8-th order) derivative stencil extended beyond the free surface using field values (indicated by the squares) on both sides of the free surface (green line). (b) Pressure field extension by 1-D Taylor expansion at the free surface from interior field values (solid) to virtual field values (dashed).*

To construct the 1-D extension for an even approximation order $M = 2K$, the wavefield is represented by an M-th order Taylor expansion at the crossing of the coordinate line for the required spatial derivative and the free surface. By assuming a 1-D wave equation in that direction, the constraints on the time derivatives of the pressure — all derivatives zero on the free surface — can be transformed into conditions on the spatial derivatives of the Taylor expansion. If we make additional assumptions of mild curvature and local invariance of the earth attributes near the free surface, it follows that all odd derivatives of the pressure field and all even derivatives of the particle velocities are zero, i.e., pressure fields must be mirrored anti-symmetrically and velocity fields symmetrically. For general 3-D topography, the resulting extension is strictly valid only in the direction normal to the free surface. Applying this extension along the coordinate directions introduces an additional numerical error, although the zero pressure at the free surface is still respected.

For example, to construct a pressure extension $p(x) = \sum_{k=0}^{K-1} a_{2k+1} x^{2k+1}$, first determine the coefficients a from

$$p_{\text{in}} = X_{\text{in}}(\alpha) a, \tag{2}$$

where $a = \begin{pmatrix} a_1 h & a_3 h^3 & \dots & a_{2K-1} h^{2K-1} \end{pmatrix}^{\mathsf{T}}$, p_{in} has the interior field values used to perform the extension, and X_{in} is a Vandermonde-type matrix depending on α, the relative distance, in terms of grid cell size h, of the first interior grid point to the free surface. Next, we can use the resulting extension to define an extrapolation operator, $E_p(\alpha)$, that maps known interior field values to the virtual values required for the derivative approximation, through

$$p_{\text{ext}} = X_{\text{ext}}(\alpha) a = X_{\text{ext}}(\alpha) X_{\text{in}}^{-1}(\alpha) p_{\text{in}} \equiv E_p(\alpha) p_{\text{in}}, \tag{3}$$

where X_{ext} has one row for each required virtual value.

The scheme sketched above is used for pressure extensions with $\alpha \geq \frac{1}{2}$ as well as all particle velocity extensions. To obtain a stable scheme, a modification is required in cases where the grid point nearest to the free surface is a pressure grid point and has $\alpha < \frac{1}{2}$. These pressure grid points are ignored in the field extension and instead, a pressure value one spacing further into the interior is used. The pressure at the ignored grid points is still needed for the derivative approximation by the 1-D stencil (see below) and, sometimes, for the derivative approximation in another coordinate direction. This can be accommodated by reconstructing such pressure values in the same way as the virtual field values, i.e., by interpolation with a local 1-D Taylor series based on neighbouring interior values and the boundary conditions.

The resulting procedure to estimate a spatial derivative, i.e., field approximation, followed by extrapolation into a virtual field, followed by application of a regular (staggered) derivative stencil, can be reformulated as the application of a modified 1-D stencil using only interior field values. This means the simulation near the topography can be based on the same propagator code as used for the rest of the domain, if it is adapted to allow for grid-dependent derivative stencils. Only the modified difference operators have to be stored. No explicit storage and application of extrapolation operators is required.

We have skipped over a number of issues. For example, for the horizontal derivatives, the coordinate lines along which derivatives are computed may cross the free surface more than once. As a result,

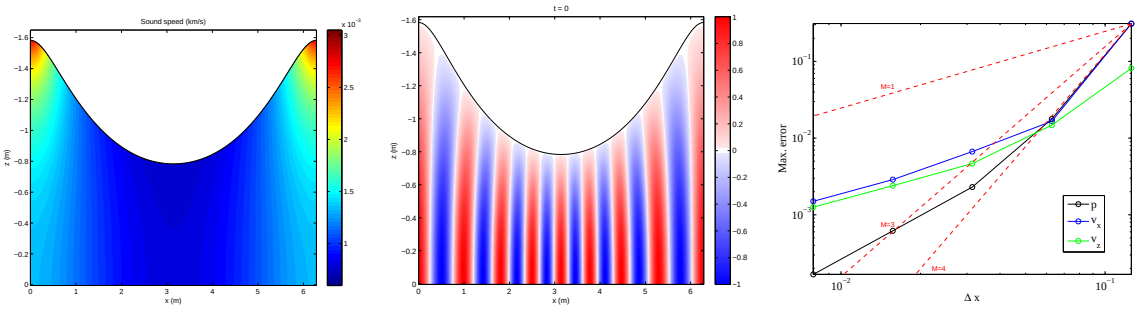

(a) (b) (c)

Figure 2 *Sound speed (a) for a 2-D test problem. The exact solution on a grid that is periodic in the horizontal direction, has a zero normal derivative for the pressure at the bottom and a zero value of the pressure at the curved surface is shown in (b). The maximum error for the test problem with a time step at half the maximum value for a discretization of order $M = 4$ as a function of grid spacing (c).*

we may not have enough interior grid points to perform the extrapolation at the requested order. To deal with this, we have implemented two strategies: (i) an automatic order reduction of the derivative operator depending on the number of available grid points, and/or (ii) an elevation regularization that flattens the topography to avoid such problematic cases. This, of course, results in a less accurate representation of the topography. Another issue is that the pressure grid points near the free surface that are implicitly reconstructed in the derivative approximation may be close to the free surface in one or two directions, but further away in another direction. For the latter direction, we then need a single, explicitly reconstructed pressure value for these 'orphan' grid points. We construct their values through a corrector operator, applied after the regular pressure update step, based on the same 1-D field approximation as before but using only the direction in which the grid point is closest to the free surface. Similarly, special care must be taken for the source injection near such corrected grid points.

The adjoint scheme is similar to the forward scheme, but since the derivative operators are no longer anti-symmetric, the modified stencils must be transposed explicitly. The same holds for the corrector operator and sampling operators for source and receivers that are positioned near the free surface. The stencil modifications do not depend on the velocity model.

Results

Figure 2 shows the sound speed for a 2-D test problem, together with the pressure at initial time. The exact solution is a traveling wave, with a zero Dirichlet boundary condition at the surface and a zero Neumann boundary condition at the bottom. The left and right boundary conditions are periodic. Panel (c) shows the maximum error after travelling around once on the periodic grid for a set of grid spacings. The dashed lines in red show the theoretical error behaviour for some orders M. In the case of an interior fourth-order spatial discretization ($M = 4$), a fourth-order error in the pressure is observed on the coarser meshes. On finer meshes, the effects of the locally 1-D approximations in the boundary conditions start to appear.

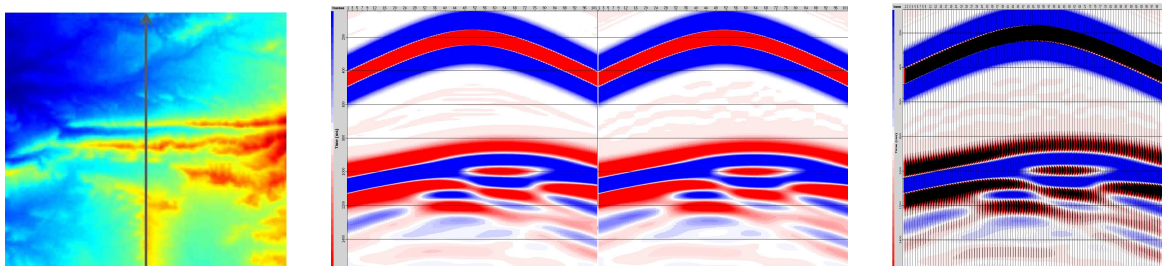

(a) (b) (c)

Figure 3 *(a) Elevation map of a 9 by 9 km area in southeastern Europe. Elevations range from 1750 to 2200 m. (b) Shot panels for a receiver line along the line indicated in (a), left: finite-difference, right: finite-element. (c) The same shot panels but overlayed, with our finite-difference approach shown as wiggles and the CML-FEM method in colour in the background.*

Figure 3 shows a comparison of our 1-D finite-difference scheme with a continuous mass-lumped finite element approach (CML-FEM, Zhebel et al., 2014) for a rough 3-D topography in southeastern Europe. Both methods were run with a 5-Hz Ricker wavelet and a constant velocity of 2500 m/s. To compare the response of the topography we have used a source at an artificial depth of 1500 m below the surface. The shot panels of Figure 3 as well as the wavefield snapshots (not shown) show a close agreement between the finite-difference and finite-element approaches.

Figure 4 shows two synthetic inversion results obtained with our scheme. For both inversions, the data were generated using a simple model with a velocity of 2000 m/s at the surface, increasing with depth with a velocity gradient of 0.6 s^{-1}. In the first experiment, the model has a horizontal free surface at zero depth. In the second, the entire model is rotated around the *y*-axis to obtain a flat free surface tilted by 30°. In both cases, we have used an initial model with a velocity gradient of 0.58 s^{-1}. We have inverted for the frequency band from 2 to 5 Hz, using offsets between 4 and 12 km.

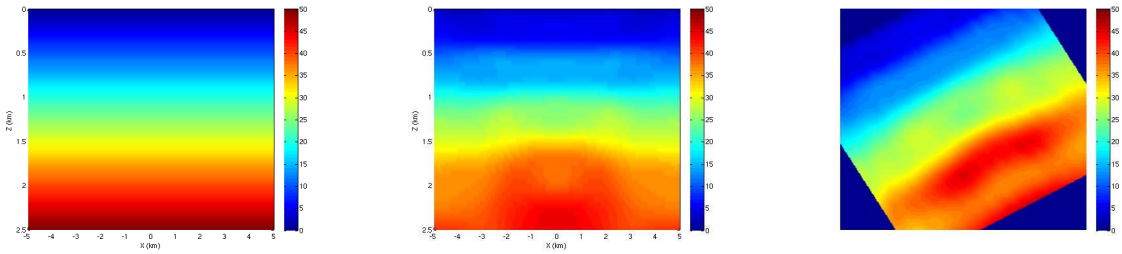

(a) (b) (c)

Figure 4 *(a) Difference between initial velocity model and the velocity model used to generate the synthetic data. (b) Velocity model update for a horizontal free surface. (c) Velocity model update for a flat free surface tilted by 30° along the x-coordinate. The size of the box is the same as the domain in (b): 10 km by 2.5 km (by 3 km out of plane).*

Conclusion

We handle 3-D topography through an immersed boundary approach that is stable for standard staggered grids as commonly used in FWI modelling codes. Since the symmetry used to obtain the 1-D field extensions is imposed along coordinate directions rather than in direction normal to the free surface, some accuracy is lost compared to a full 3-D extension. The resulting approach is relatively simple to implement, affordable and, for the acoustic wave equations investigated, sufficiently accurate.

References

Bohlen, T. and Saenger, E. [2006] Accuracy of heterogeneous staggered-grid finite-difference modeling of Rayleigh waves. *Geophysics*, **71**, 109–115.

Brossier, R., Diaz-Mojica, J., Beller, S. and Pajot, B. [2014] 3D elastic wave modeling for exploration scale Full Waveform Inversion. Tech. Rep. 78, Seiscope.

Hestholm, S. [2003] Elastic wave modeling with free surfaces: stability of long simulations. *Geophysics*, **68**, 314–321.

Komatitsch, D. and Vilotte, J. [1998] The spectral element method: an efficient tool to simulate the seismic response of 2-D and 3-D geological structures. *Bulletin of the Seismological Society America*, **88**, 368–392.

Lombard, B., Piraux, J., Gélis, C. and Virieux, J. [2008] Free and smooth boundaries in 2-D finite-difference schemes for transient elastic waves. **172**(1), 252–261.

De la Puente, J., Ferrer, M., Hanzich, M., Castillo, J.E. and Cela, J.M. [2014] Mimetic seismic wave modeling including topography on deformed staggered grids. *Geophysics*, **79**(3), T125–T141.

Robertsson, J. [1996] A numerical free-surface condition for elastic/viscoelastic finite-difference modeling in the presence of topography. *Geophysics*, **61**, 1921–1934.

Zhebel, E., Minisini, S., Kononov, A. and Mulder, W.A. [2014] A comparison of continuous mass-lumped finite elements with finite differences for 3-D wave propagation. *Geophysical Prospecting*, **62**(5), 1111–1125.